JACC: BASIC TO TRANSLATIONAL SCIENCE VOL. 3, NO. 1, 2018

PRECLINICAL RESEARCH

Rapid Endothelialization of Off-the-Shelf Small Diameter Silk Vascular Grafts

Elysse C. Filipe, MSc,[a,b] Miguel Santos, MSc,[a,b] Juichien Hung, MSc,[a] Bob S.L. Lee, MSc,[a,b] Nianji Yang, MPHIL,[a,b] Alex H.P. Chan, BSc,[a,b] Martin K.C. Ng, MD, PHD,[a,c] Jelena Rnjak-Kovacina, PHD,[d] Steven G. Wise, PHD[a,b]

VISUAL ABSTRACT

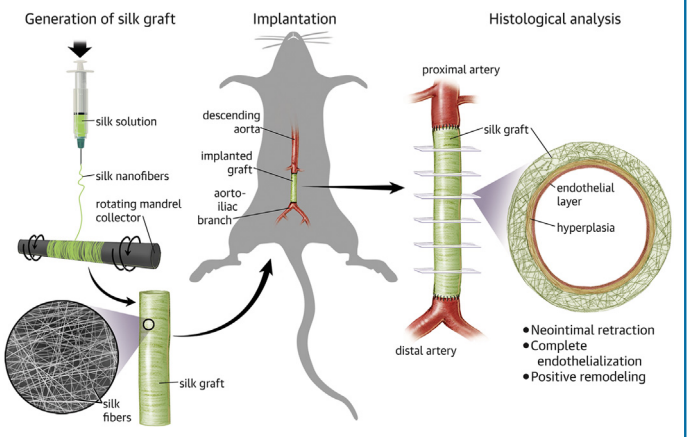

Filipe, E.C. et al. J Am Coll Cardiol Basic Trans Science. 2018;3(1):38–53.

Electrospinning of silk to create nanofibers, which deposit onto a rotating collector. This results in the formation of a pure silk conduit of 1.5 mm internal diameter. These conduits are then implanted into the descending abdominal aorta of Sprague Dawley Rats with end-to-end suturing, and left for 3, 6, 12, and 24 weeks. Endpoint histologic analysis of the explanted grafts demonstrate hyperplasia stabilization, complete endothelialization and excellent blood compatibility.

HIGHLIGHTS

- ***Bombyx mori* silk was electrospun to engineer mechanically robust vascular grafts that support endothelial cell attachment and monolayer formation while resisting blood adhesion and fibrin assembly in vitro.**
- **Silk grafts were evaluated in a rat aortic interposition grafting model at 3, 6, 12, and 24 weeks. Graft survival for silk grafts (95%) was superior to control ePTFE (73%) at 24 weeks.**
- **Comprehensive histologic analysis of the grafts demonstrated near complete endothelialization by 6 weeks, which occurred concomitantly with neointima regression, characterized by a loss in cellularity, a phenotypic switch in SMC and an increased ECM expression.**
- **Silk grafts appear to undergo positive remodeling over time, with temporal reductions in apoptotic and inflammatory cells, adventitial granulation tissue, and the deposition of new ECM proteins.**

From the [a]Applied Materials Group, The Heart Research Institute, Sydney, New South Wales, Australia; [b]Sydney Medical School, University of Sydney, Sydney, New South Wales, Australia; [c]Department of Cardiology, Royal Prince Alfred Hospital, Camperdown, New South Wales, Australia; and the [d]Graduate School of Biomedical Engineering, University of New South Wales-Sydney, Sydney, New South Wales, Australia. This work was supported by the National Health and Medical Research Council (APP1066174; Dr. Ng) and an Australian Research Council grant (DP150104242; Dr. Rnjak-Kovacina). Ms. Filipe is a recipient of an Australian Postgraduate Scholarship. Mr. Santos has received funding support from The Heart Research Institute. Financial support was received from E. Brackenreg. All other authors have reported that they have no relationships relevant to the contents of this paper to disclose.

All authors attest they are in compliance with human studies committees and animal welfare regulations of the authors' institutions and Food and Drug Administration guidelines, including patient consent where appropriate. For more information, visit the *JACC: Basic to Translational Science* author instructions page.

Manuscript received June 30, 2017; revised manuscript received December 13, 2017, accepted December 15, 2017.

ISSN 2452-302X https://doi.org/10.1016/j.jacbts.2017.12.003

SUMMARY

Synthetic vascular grafts for small diameter revascularization are lacking. Clinically available conduits expanded polytetrafluorethylene and Dacron fail acutely due to thrombosis and in the longer term from neointimal hyperplasia. We report the bioengineering of a cell-free, silk-based vascular graft. In vitro we demonstrate strong, elastic silk conduits that support rapid endothelial cell attachment and spreading while simultaneously resisting blood clot and fibrin network formation. In vivo rat studies show complete graft patency at all time points, rapid endothelialization, and stabilization and contraction of neointimal hyperplasia. These studies show the potential of silk as an off-the-shelf small diameter vascular graft. (J Am Coll Cardiol Basic Trans Science 2018;3:38–53)

ABBREVIATIONS AND ACRONYMS

ECM = extracellular matrix

ePTFE = expanded polytetrafluoroethylene

PCL = polycaprolactone

PCNA = proliferating cell nuclear antigen

SMC-α = smooth muscle cell actin

vWF = von Willebrand factor

In the absence of appropriate autologous grafts, revascularization of ischemic tissue is reliant on the availability of effective synthetic conduits. In applications in the coronaries and lower limbs, where diameters are <6 mm, current synthetic graft materials uniformly fail, driving significant research in bioengineering, aiming to generate viable alternatives (1,2).

However, more than 2 decades of research has failed to provide the ideal platform for engineering of small diameter synthetic conduits for clinical use. A significant proportion of preclinical research has used vascular cells as a tool to produce a native scaffold, rich in extracellular matrix (ECM) components. This is frequently in conjunction with lengthy maturation phases ex vivo (1,2). The most successful have demonstrated feasibility in large animal models (3–9). However, the use of cell-containing scaffolds or cell by-product scaffolds poses a significant limitation to the clinical translatability of such approaches, both logistically and financially. The most promising approach to bioengineered conduits are decellularized before use to reduce immunogenicity and improve translation. A recent phase II human trial has demonstrated the clinical feasibility of this approach, but additional studies of efficacy are still required (9). Similarly, traditional polymeric scaffolds such as polyurethane have also failed to improve clinical outcomes due to unexpected degradation in vivo, pro-inflammatory by-products, and poor interactions with vascular cells (1,10,11). Therefore, there remains a significant unmet need for new materials for synthetic vascular conduits that combine favorable mechanical properties and compatibility with vascular cells and blood, which can be readily translated to the clinic.

Bombyx mori (silkworm) silk fibroin (referred to as "silk") is a naturally occurring protein polymer with unique mechanical and physical characteristics, which make it a widely used biomaterial. It has a long history in applications as diverse as skin repair, retina replacement, and clinically as sutures (12). Recent methodological advances in silk processing have significantly improved silk fibroin purity reducing the inflammation that has been considered a weakness of silk in the past (13). In addition, advancements in silk processing and manufacturing methods have made the production of mechanically robust conduits feasible, leading us to revisit a well-established biomaterial for vascular repair applications (12,14). In this work, we demonstrate the engineering of a silk conduit, electrospun from water and cross-linked with water vapor, thus eliminating the use of potentially toxic chemical precursors. Silk conduits manufactured in this way have tunable physical properties and high vascular compatibility in vitro and were assessed in a rat model of abdominal aortic replacement. Our conduits demonstrate excellent surgical handling and in vivo patency for up to 6 months with near-complete endothelialization as early as 6 weeks with concomitant stabilization and contraction of neointimal hyperplasia. Silk grafts appear to undergo positive remodeling over time, with temporal reductions in apoptotic and inflammatory cells, adventitial granulation tissue, and the deposition of new ECM proteins. Overall, this work demonstrates the robust in vivo performance of a cell-free silk scaffold for use as a small diameter vascular graft, a simple, cost-effective platform designed to be readily translated for broader clinical use.

METHODS

Full methods are included in the Supplemental Appendix.

IN VIVO RAT MODEL OF AORTIC REPLACEMENT. Study approval was obtained from the Sydney Local Health District Animal Welfare Committee (protocol number 2014/028). Experiments were conducted in accordance with the Australian Code of Practice for the

Care and Use of Animals for Scientific Purpose. Briefly, electrospun silk grafts were prepared and disinfected in 70% ethanol with exposure to ultraviolet light for 30 min. Samples were stored in air until the time of surgery. Expanded polytetrafluoroethylene (ePTFE) was purchased from Bard Scientific (Covington, Georgia) and stored in air until the time of surgery. Forty-three 8-week-old male rats (Sprague Dawley) were purchased from Laboratory Animal Service (New South Wales, Sydney Australia). Rats were given a single intramuscular injection of ketamine (75 mg/kg) and medetomidine (0.5 mg/kg) to induce anesthesia. The abdomen was shaved and a midline laparotomy incision was performed. The infrarenal abdominal aorta was exposed and clamped proximally, just below the renal arteries, and distally, just above the aortoiliac bifurcation. The abdominal aorta was resected and a 0.8-cm section of silk or ePTFE ($n = 21$ and 22 for silk and ePTFE, respectively) was implanted with 8 interrupted 9-0 silk sutures at each anastomosis. After re-establishment of blood flow, the abdominal cavity and overlying skin were sutured closed. At the end of surgery, rats were given atipamezole (in equal volume to medetomidine; intramuscularly) to reverse the anesthesia. For pain management, temgesic (buprenorphine 2 mg/kg body weight) was provided once a day for 24 to 48 h. Animals were kept on normal food and water ad libitum for the duration of the study and no ongoing anticoagulants were given. Rats were followed up for 3, 6, 12, and 24 weeks ($n = 5$ per time point) at which time, animals were anesthetized (as described) and the graft excised for scanning electron microscopy and histologic analysis.

HISTOLOGIC STAINING AND IMMUNOHISTOCHEMISTRY. On explantation, all samples were fixed in 4% paraformaldehyde, overnight. Samples were then processed for scanning electron microscopy imaging or histologic analysis by paraffin processing and embedding (Leica Microsystems, Wetzlar, Germany). Graft cross sections, from distal to proximal were cut. For staining, slides from 6 equidistant points throughout the graft were deparaffinized and immediately stained with hematoxylin and eosin, Milligan trichrome for collagen deposition, orcein for detection of elastin, or alcian blue for detection of proteoglycans. For immunohistochemistry, slides were deparaffinized and subject to heat-mediated antigen retrieval prior to permeabilization and blocking with 10% goat serum. Primary antibodies (rabbit α-von Willebrand factor [vWF] [Dako, Agilent, Santa Clara, California]; rabbit α-proliferating cell nuclear antigen [PCNA] [Abcam, Cambridge, United Kingdom]; rabbit α-CD34 [Abcam]; rabbit α-CD68 [Abcam]; rabbit α-vimentin [Abcam]; rabbit α-caspase [Cell Signaling Technology, Danvers, Massachusetts]; mouse α-smooth muscle cell actin [SMC-α] fluorescein isothiocyanate [Sigma-Aldrich, St. Louis, Missour]) were incubated at a dilution of 1:250 in antibody diluent (Dako). Secondary antibody (goat α-rabbit Alexa 594 [Abcam]) was incubated at 1:250 in antibody diluent, after which NucBlue (Invitrogen, Thermo Fisher Scientific, Waltham, Massachusetts) was used to detect cell nuclei. Slides were coverslipped in anti-fading medium (Dako) and imaged in the Zeiss Axioscan (Jena, Germany) at 20× magnification.

IMAGE ANALYSIS. All image analyses were performed in Image Pro Premier (version 9.2, Media Cybernetics, Inc., Rockville, Maryland), where a minimum of 3 sections were analyzed per region (distal to proximal) per graft for each stain. For endothelialization analysis, vWF and CD34-positive portions of the luminal cross sections were measured and are represented as percentage of endothelialization relative to the total circumference of the lumen of the same section. For hyperplasia and granulation tissue analysis, the neointimal and adventitial tissue areas were calculated and are represented as a percentage relative to the total lumen size of the graft in each section. For quantification of $CD68^+$ cells, the amount of red staining was quantified in the granulation tissue and is represented as an absolute pixel value. Collagen analysis was performed by calculating the area of collagen (aqua/blue) and cells (purple) and is represented as a ratio of collagen to cells in each section. Elastin analysis was performed by calculating the total area of positive elastin staining (dark purple) and is represented as a percentage elastin relative to the total hyperplasia region of each section. Quantification of proteoglycans was performed by calculating the amount of positive (aqua/blue) staining, relative to the total hyperplasia region of each section. The SMC-α/PCNA double stain was analyzed by quantifying the total green and red areas of the hyperplasia, respectively, and data are represented as percentage of positive green or red staining relative to the total stained area in the hyperplasia per section.

STATISTICAL ANALYSIS. Data are expressed as mean ± SEM and statistical analysis was performed using GraphPad Prism 7 version 7.02 for Windows (GraphPad Software Inc., San Diego, California). The normal distribution of our data sets was confirmed using the Kolmogorov-Smirnov test and parametric analysis was performed. Where appropriate, data were analyzed by unpaired Student's *t*-test when comparing 2 samples and analysis of variance when

FIGURE 1 **Mechanical Properties of Electrospun Silk Scaffolds for Vascular Grafting**

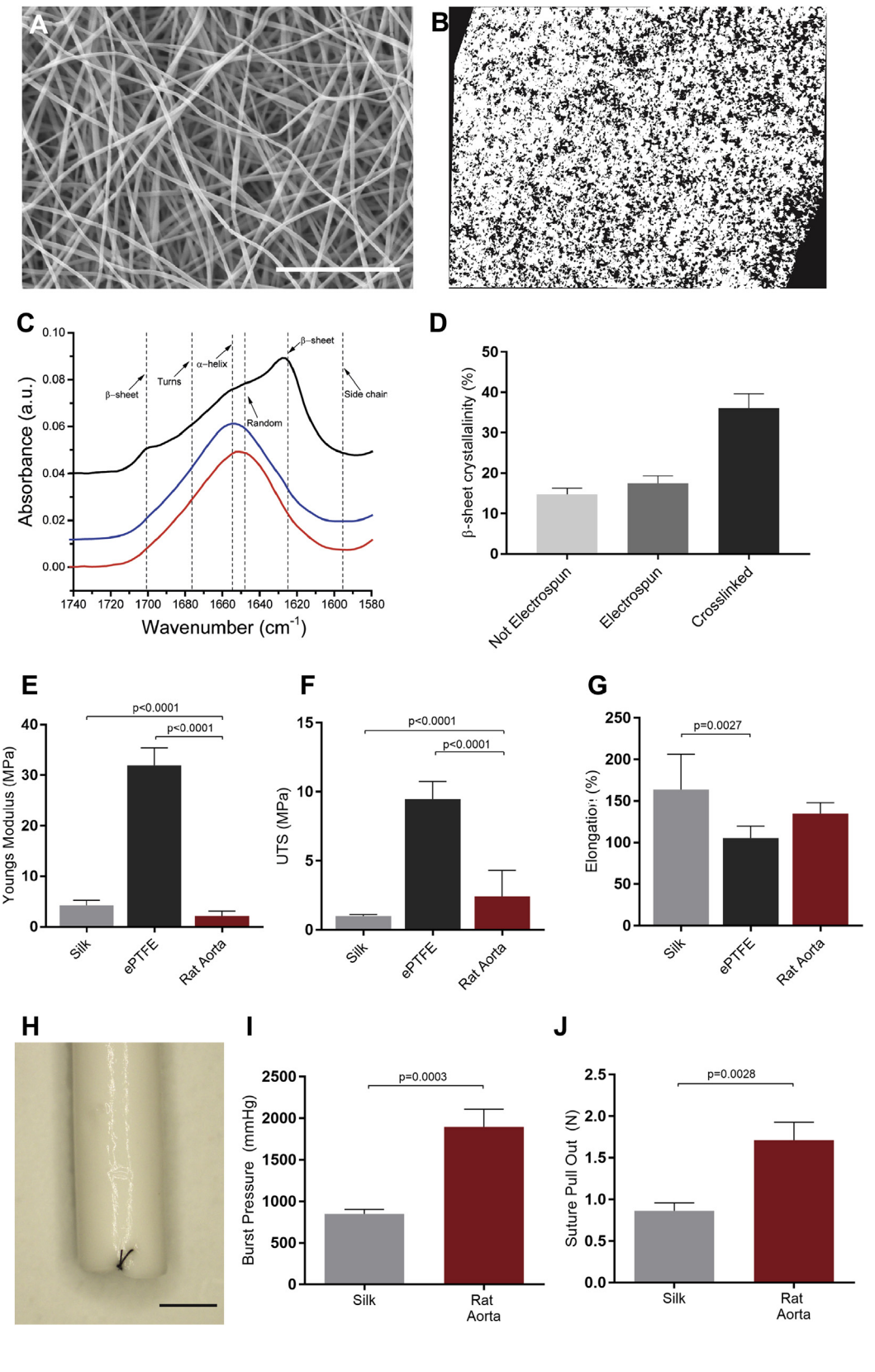

Continued on the next page

comparing multiple samples. Post hoc comparisons were analyzed with Tukey multiple comparisons test. For analysis of **Figures 5E, 6C, 6D, 7C, 7D and** Supplemental Figures 4B, 6B, and 7B, 1-way analysis of variance was performed on the group averages (represented as a dashed line for each time point). For group averages, all points throughout the graft were averaged for each animal (n = 4 animals). The survival of grafts over time was assessed using Kaplan-Meier survival curve analysis with a Mantel-Cox test. We considered p values <0.05 to be significant.

RESULTS

SILK SCAFFOLDS PROVIDE APPROPRIATE MECHANICAL PROPERTIES FOR USE AS A VASCULAR GRAFT MATERIAL. Electrospun silk scaffolds (**Figure 1A**) demonstrated an average fiber diameter of 355 ± 5.0 nm and a relative porosity of 23.3 ± 1.2% (**Figure 1B**). The overall β-sheet crystallinity of the silk fibroin was unaffected by the electrospinning process and was increased on cross-linking, from 17.58% to 36.08%, inducing water insolubility (**Figures 1C and 1D**). The mechanical properties of the electrospun silk scaffolds were evaluated in comparison to commercial ePTFE and native rat aorta. The elasticity of the scaffolds was determined by the slope of the linear region of the stress/strain curve of each replicate sample. Electrospun silk scaffolds revealed a Youngs modulus of 4.2 ± 0.5 MPa, not significantly higher than the native rat aorta (2.1 ± 1.0 MPa), and 7.6-fold more elastic than ePTFE (31.9 ± 1.3 MPa) (**Figure 1E**). Similarly, the ultimate tensile strength of the silk scaffolds (1.0 ± 0.03 MPa) were more similar to rat aorta (2.4 ± 1.87 MPa) than ePTFE (9.5 ± 0.47 MPa) (**Figure 1F**). Finally, elongation data found that the silk scaffolds tolerated an increased stretch before breakage (163 ± 11.7%) when compared with the ePTFE grafts (105 ± 5.5%), albeit not significantly different to the native rat aorta (134 ± 13.2%) (**Figure 1G**). Silk scaffolds were then engineered into small diameter (1.5-mm) grafts (**Figure 1H**) for analysis of graft-specific mechanical properties. Burst pressure analysis further demonstrated the strength of the silk grafts that burst at an average of 849 ± 59 mm Hg. Although the values obtained were less than those for the native rat aorta (1,896 ± 260 mm Hg), they were in large excess of physiological blood pressure (**Figure 1I**). Suture retention studies showed that the silk grafts withstood an average 0.86 ± 0.1 N of force before tearing (**Figure 1J**). These values were below those of the native rat aorta (1.71 ± 0.3 N), but superior to previously published data for other synthetic graft materials (15).

ENDOTHELIAL CELLS FORM A MONOLAYER ON SILK SCAFFOLDS IN VITRO WITH EXCELLENT BLOOD COMPATIBILITY. We next sought to evaluate both endothelial cell and blood compatibility on electrospun silk scaffolds. Endothelial cells rapidly attached to and spread on the surface of the silk scaffolds, after just 3 h in culture (**Figure 2A**). The same cells on ePTFE remained poorly attached and did not spread on the surface (**Figure 2B**). Longer time points of 1, 3, and 6 days showed an increase in cell density on the silk scaffolds, with cells maintaining a spread-out morphology (**Figure 2C**). In contrast, the endothelial cells on ePTFE remained poorly attached even at 6 days post-seeding (**Figure 2D**). Endothelial cell seeding and subsequent cross-sectioning of the silk scaffolds demonstrated the formation of a monolayer on the surface, without penetrating the silk scaffold (**Figure 2E**). Further vascular endothelial cadherin immunostaining of confluent endothelial cells confirmed the formation of tight junctions between the seeded cells, indicative of a nonpermeable endothelial barrier (**Figure 2F**). Conversely, cells on ePTFE were unable to form these junctions (**Figure 2G**).

Blood compatibility assays also demonstrated the favorable blood compatibility of electrospun silk scaffolds. Polycaprolactone (PCL) was chosen as a control for electrospun scaffolds, as this polymer yields a material with similar fibrous morphology to the electrospun silk and which has been well validated as a synthetic graft material (16,17). Contact with platelet-rich plasma enriched with fluorescent

FIGURE 1 Continued

(A) Scanning electron micrograph of electrospun silk. Scale bar = 10 μm. **(B)** Cross section of electrospun silk **(white),** demonstrating scaffold porosity **(black). (C)** Representative amine I Fourier transform infrared spectroscopy spectra of silk prior to electrospinning **(red),** post-electrospinning **(blue)**, and after cross-linking **(black). (D)** Proportion of β-sheet crystallinity in electrospun silk prior to electrospinning, post-electrospinning, and after cross-linking. Mechanical properties of silk, compared with expanded polytetrafluoroethylene (ePTFE) and fresh rat aorta as control scaffolds. **(E)** Youngs moduli, **(F)** ultimate tensile strength (UTS), and **(G)** percentage of elongation. Data are mean ± SEM; n = 9 to 12 (n = 2 for rat aorta). **(H)** Macroscopic images of electrospun silk graft. Scale bar = 1 mm. **(I)** Quantification of the maximum pressure before failure. Data are mean ± SEM; n = 6 (n = 3 for rat aorta). **(J)** Suture pull-out data of silk graft, with rat aorta as a control. Data are mean ± SEM; n = 7 (n = 3 for rat aorta).

FIGURE 2 **Endothelial Cell and Blood Compatibility With Electrospun Silk Scaffolds for Vascular Grafting**

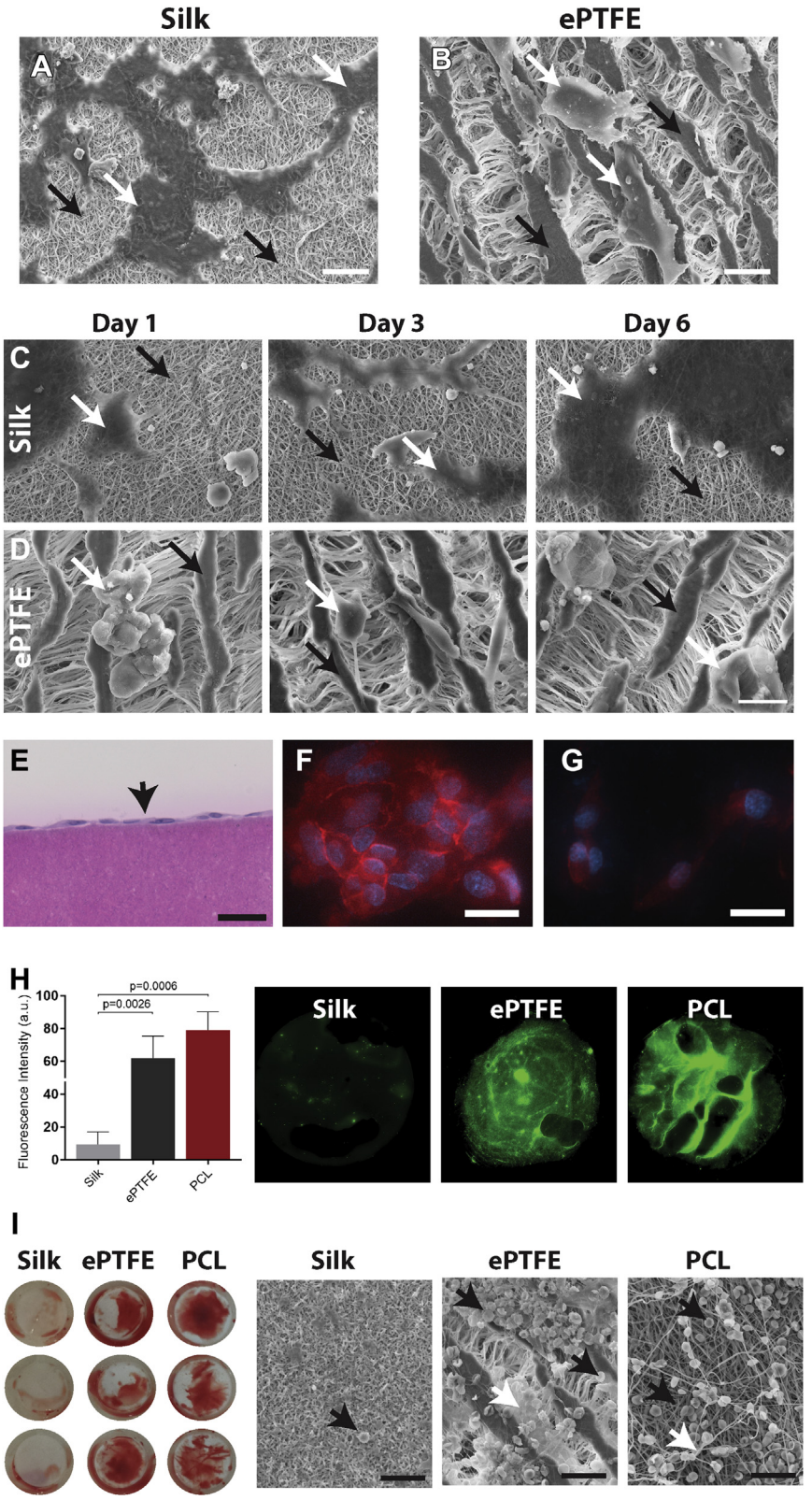

Continued on the next page

fibrinogen demonstrated negligible fibrin network formation on the surface of the electrospun silk, while both the ePTFE and electrospun PCL control scaffolds displayed extensive fibrin networks at the same time point (**Figure 2H**). Quantification of the fluorescence intensity confirmed 6.6- and 7.8-fold less staining on electrospun silk when compared with that of ePTFE and PCL, respectively. Contact with whole blood further validated these results, with macroscopic images demonstrating the complete absence of clot formation on silk, while significant clot formation was visible on both control scaffolds. Scanning electron microscopy confirmed this, with almost no red blood cells on the surface of silk. The ePTFE and PCL scaffolds displayed extensive red blood cell deposition (**Figure 2I**, black arrow) with clear fibrin network formation in the latter (**Figure 2I**, white arrow).

SILK GRAFTS DISPLAY HIGH PATENCY AT 6 MONTHS IN A RAT. Having confirmed appropriate mechanical and biological compatibilities of the silk scaffolds, small diameter silk grafts were implanted into the abdominal aorta of Sprague Dawley rats (**Figures 3A and 3B**). Control animals were implanted with commercial ePTFE of similar diameter (**Figure 3C**). Silk scaffolds demonstrated excellent handling and were successfully implanted in all animals, with explantations performed at 3, 6, 12, and 24 weeks. Graft survival was 95% (20 of 21) for the silk grafts, with only 1 death within 24 h of the implantation (**Figure 3D**). However, ePTFE failure was higher at 27% (6 of 22) with graft failures relating to deaths occurring postoperatively ($n = 2$) or, alternatively, at the explantation time point of 3 ($n = 2$) and 6 weeks ($n = 2$) due to complete occlusion (Supplemental Figure 1). These results demonstrate a high degree of variability in ePTFE survival, which is consistent with observations in humans (18).

RAPID ENDOTHELIALIZATION, COMPLETE BY 12 WEEKS. The rate of endothelialization following injury is a critical determinant of vascular lesion formation and areas of injury that rapidly endothelialize have significantly less intimal thickening and stenosis, while also deterring thrombus formation (19). To evaluate this, we first performed scanning electron microscopy of the luminal side of the grafts at each explantation time point. The images reveal that silk grafts have complete cell coverage as early as 3 weeks, with no underlying silk visible (**Figure 4A**), a feature that is maintained at all later time points. Higher magnification further showed a rough cobblestone cell morphology at 3 weeks, changing to a more elongated morphology by 6 weeks (**Figure 4B**). The resolution of the images was not sufficient to allow more detailed morphological analysis of the cells. Conversely, the scanning electron micrographs of the ePTFE grafts revealed a bare surface, with the underlying material morphology clearly visible at 3 and 6 weeks (**Figures 4C and 4D**). At later time points of 12 and 24 weeks, focal points of cell coverage were observed; however, large areas of uncovered ePTFE remained. Immunohistochemistry of graft cross sections with vWF was performed to quantify endothelial cell presence, which is consistent with multiple previous studies (3,4,8,15,20). Silk graft cross sections showed endothelial cells present as early as 3 weeks, with complete coverage of anastomotic regions by 6 weeks and full endothelialization by 12 weeks (**Figures 5A and 5B**). The vWF staining of the ePTFE graft cross sections was confounded by significant non-endothelial cell-specific staining, particularly at earlier time points. This may be due to physical collection in the porous graft wall, as previously reported (21) (Supplemental Figure 2). Additional staining for CD34+ endothelial progenitor cells was also performed to establish the contribution of these cells to endothelialization (17). Results show $CD34^+$ staining throughout the length of silk grafts as early as 3 weeks (Supplemental Figure 3A). This was shown to increase at later time points, consistent with the vWF data (Supplemental Figure 3B). Overall, the degree of $CD34^+$ staining was lower than for vWF, suggesting that although these cells contribute to

FIGURE 2 Continued

Representative scanning electron micrograph images of endothelial cell attachment on electrospun silk scaffolds **(A)** and expanded polytetrafluoroethylene (ePTFE) control scaffolds **(B).** Scale bar = 20 μm. Representative scanning electron micrograph images of endothelial cells on electrospun silk **(C)** and ePTFE scaffolds **(D)** at 1, 3, and 6 days post-seeding. Scale bar = 20 μm. **(A to D) White arrows** demonstrate cells and **black arrows** show scaffold surface. **(E)** Representative cross-sectional image of an endothelial cell monolayer on the surface of electrospun silk. Scale bar = 50 μm. vascular endothelial cadherin staining of endothelial cells on the surface of electrospun silk **(F)** and ePTFE **(G).** Scale bar = 25 μm. **(H)** Quantification of fluorescent fibrinogen on silk, polycaprolactone (PCL), and ePTFE scaffolds. Representative images of the scaffolds demonstrating fibrin network formation in **green. (I)** Macroscopic images of the whole blood assay on silk, PCL, and ePTFE scaffolds. Representative scanning electron micrograph images of these same scaffolds revealing red blood cells **(black arrows)** and fibrin deposition **(white arrows)** on the different scaffolds. Scale bar = 25 μm.

FIGURE 3 **In Vivo Experimental Design in a Rat Model of Abdominal Aortic Replacement**

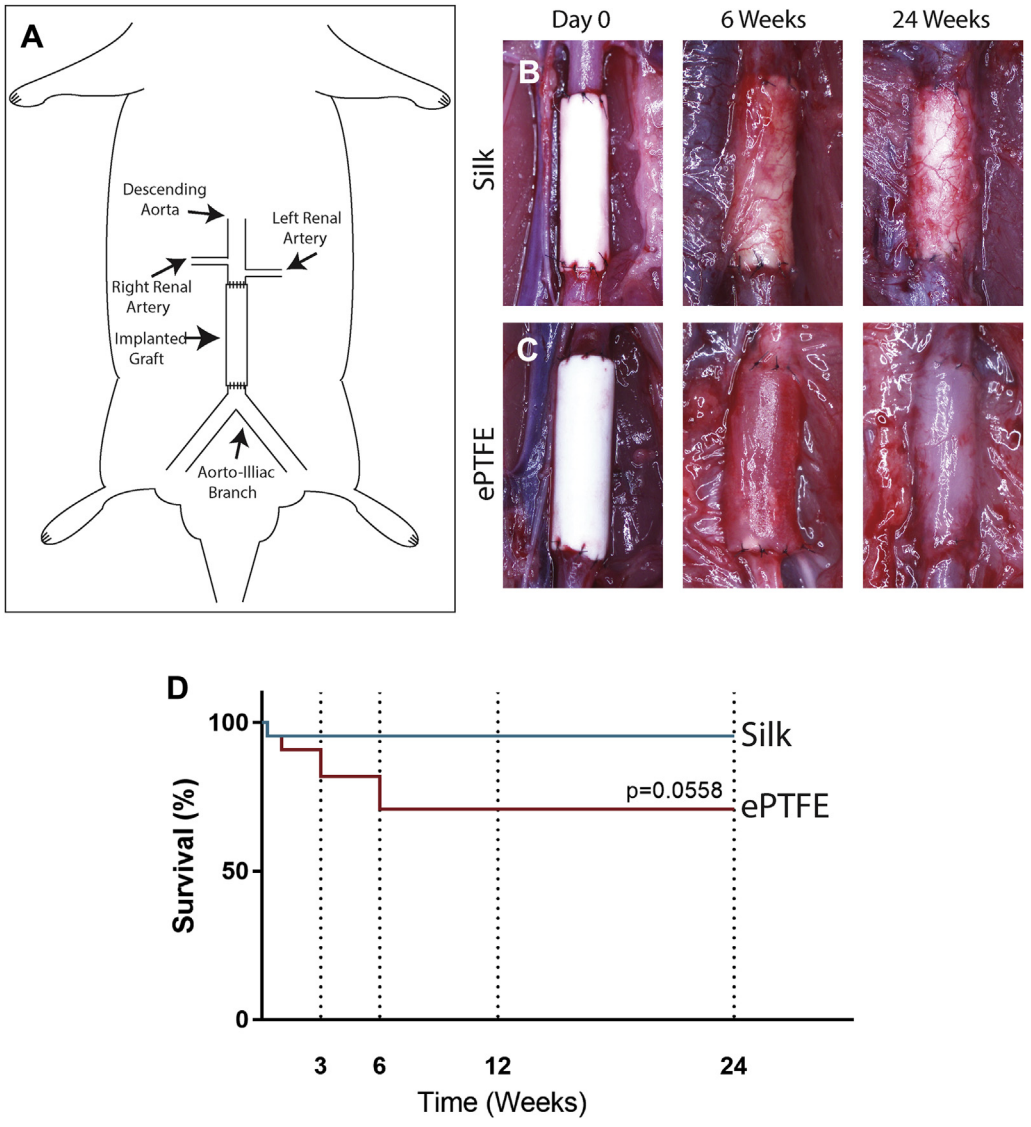

(A) Schematic of in vivo implantation procedure in rat. **(B)** Silk and **(C)** expanded polytetrafluoroethylene (ePTFE) control grafts at implantation and at the explantation time points of 6 and 24 weeks. **(D)** Kaplan-Meier curve depicting graft survival of silk **(blue)** and ePTFE **(red)**. n = 21 and 22 for silk and ePTFE grafts, respectively.

endothelialization, additional mechanisms, including transmigration are also playing a role (22).

SMC-DRIVEN NEOINTIMAL HYPERPLASIA STABILIZES AND CONTRACTS BY 6 WEEKS IN VIVO. The major driver of long-term graft failure is neointimal hyperplasia within the graft lumen. We extensively characterized this by evaluating the extent of neointimal formation over time, while also investigating the phenotype of the SMC present. Hematoxylin and eosin staining of the graft cross sections demonstrated the characteristic bell-shaped neointima distribution from distal to proximal throughout the graft, with greater amounts observed at the anastomotic regions (**Figures 6A and 6C**). At 6 weeks, however, hyperplasia was equal throughout the graft length at an average 40.9 ± 3.8%. Interestingly, hyperplasia at later time points was reduced to 27.9 ± 1.9% and 27.0 ± 0.3% at 12 and 24 weeks, respectively. These data suggest that hyperplasia stabilizes by 6 weeks, corresponding to when

FIGURE 4 Scanning Electron Microscopy of Silk and ePTFE Grafts at Explantation

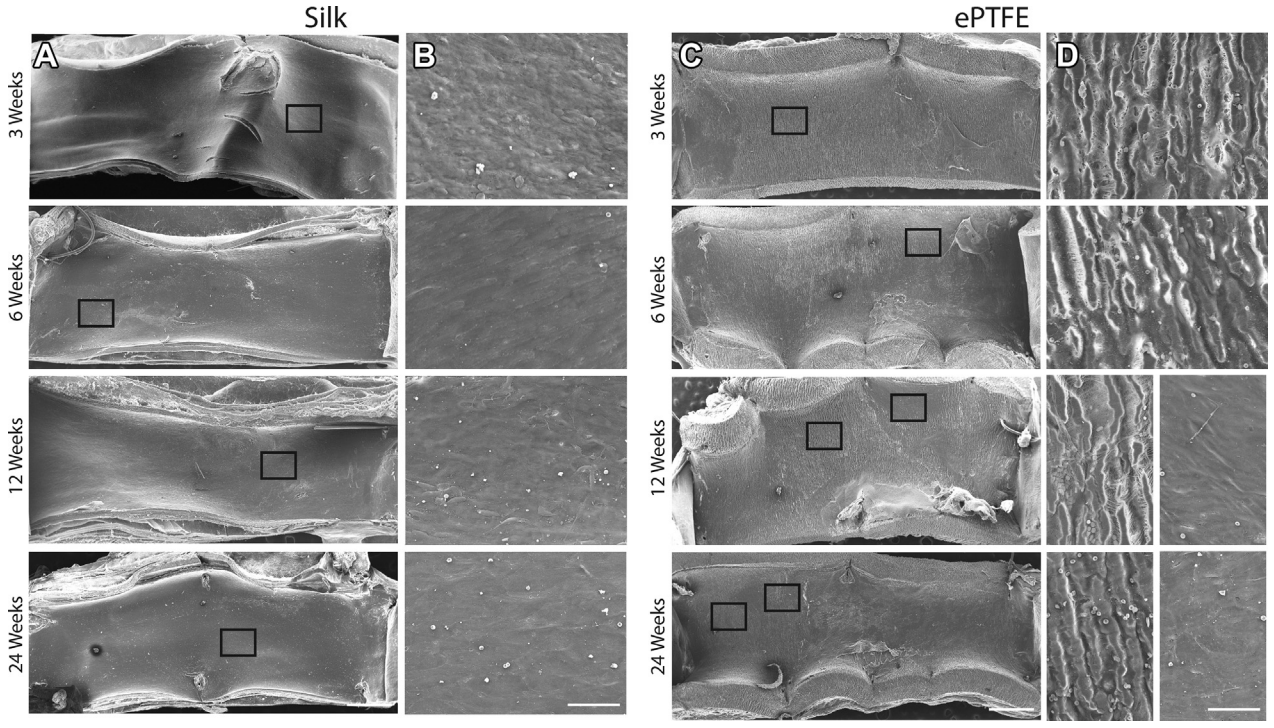

Scanning electron micrograph images of explanted silk **(A)** and expanded polytetrafluoroethylene (ePTFE) **(C)** grafts at 3, 6, 12, and 24 weeks. Scale bar = 500 μm. Representative high magnification images **(black boxes in A and C)** of silk **(B)** and ePTFE **(D).** Scale bar = 50 μm.

endothelialization is also almost complete and potentially contributing to the reduced proliferation of SMC. This phenomenon has been called neointimal retraction and is similarly observed in cases of human stent implantation (23,24), generally at later time points of >18 months.

To better understand the change in hyperplasia composition over time, we evaluated ECM deposition (collagen, elastin, and proteoglycans) and SMC phenotype. Milligan trichrome staining of the graft cross sections revealed a loosely packed collagen matrix with abundant cell presence at 3 weeks (Supplemental Figure 4). This abundance of cells was lost at later time points, with extensive and compact collagen detected instead. Staining of caspase-3^{+} apoptotic cells, evident at early time points but reducing over time (Supplemental Figure 5A), demonstrates cell death consistent with this overall loss. The progressive loss of cells is similarly observed in stented human samples where a decrease in SMC is accompanied by a regression in percentage stenosis, the point at which some investigators suggest healing is complete (23,24). Orcein staining of the graft cross sections showed increasing levels of elastin secretion in the hyperplasia, with greater amounts detected at longer time points (Supplemental Figure 6). Elastin secretion by SMC has been attributed to a contractile SMC phenotype (23,25), suggesting an increased presence of mature SMC in the hyperplasia layer at these later time points. Alcian blue staining also demonstrated increasing levels of proteoglycans in the hyperplasia, particularly in the mid-section of the graft, where levels increase by more than 5-fold from 3 to 24 weeks. Similarly to elastin, proteoglycans are recognized as important regulators of SMC phenotype, promoting maintenance of contractile phenotype and reducing SMC proliferation (Supplemental Figure 7) (26). Finally, a double-stain immunohistochemistry for PCNA, a proliferation marker, and SMC-α, a marker for mature SMC, was performed to evaluate the proportion of proliferative/stable SMC in the hyperplasia layer. The results clearly demonstrate a phenotypic switch in the cells that at early time points are mainly PCNA^{+}, but at later time points (from 12 weeks) reveal a dominance of SMC-α^{+} cells (**Figures 6B and 6D**). These results indicate the increasing stability of the neointima that initiates as early as week 6 post-implantation.

FIGURE 5 **Immunohistologic Staining for vWF^{+} Cells in Silk Grafts at Explantation**

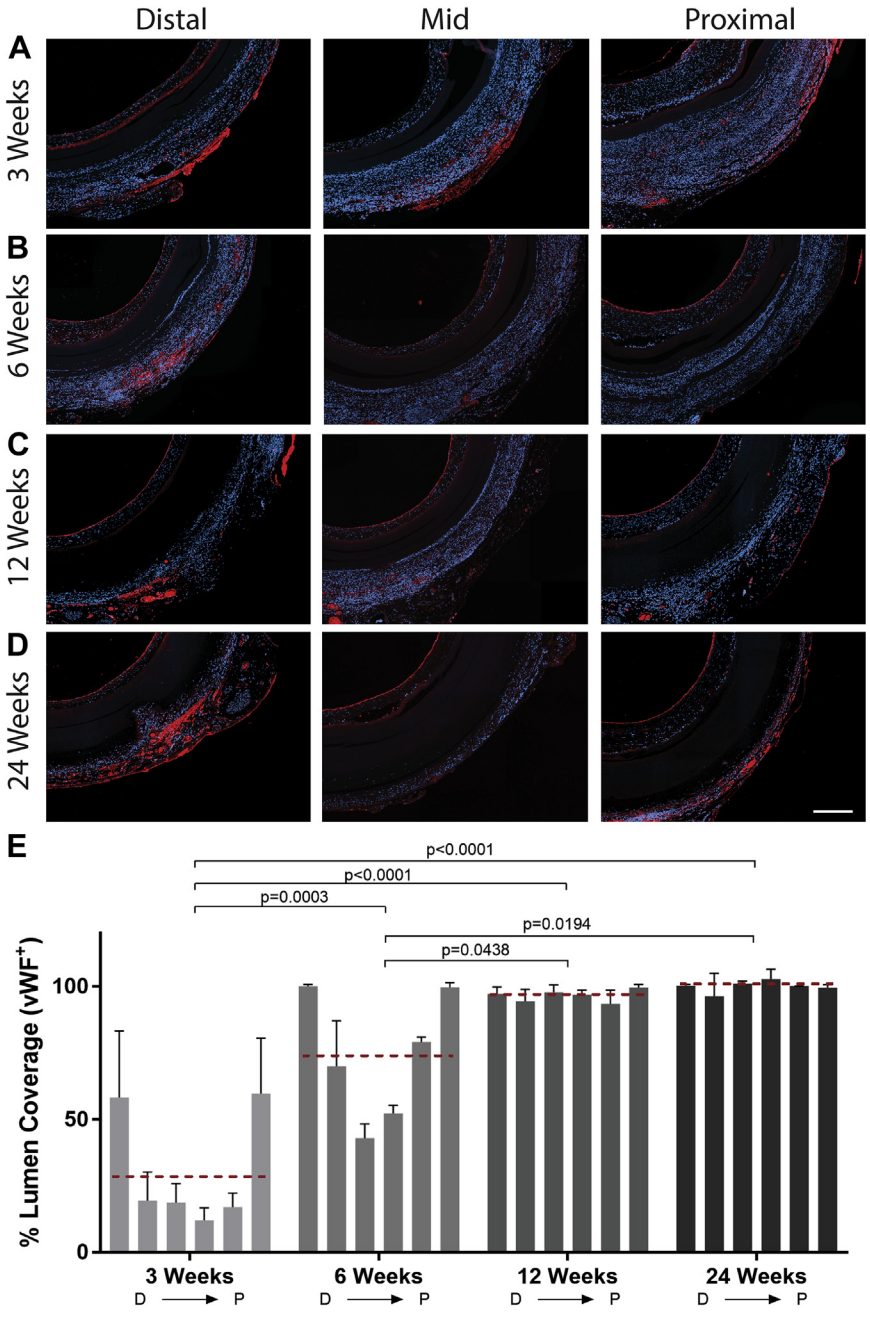

Representative micrograph images of von Willebrand factor (vWF) immunohistochemistry staining on cross sections of silk grafts at 3 **(A)**, 6 **(B)**, 12 **(C)**, and 24 **(D)** weeks. vWF staining is **red,** and 4′,6-diamidino-2-phenylindole staining is **blue.** Scale bar = 200 μm. **(E)** Quantification of vWF coverage on the lumen of the graft depicting vWF positivity as early as 3 weeks and complete coverage by 12 weeks. N = 4 animals per time point with 3 images analyzed per region per graft. The **red dashed line** indicates the average vWF^{+} staining for each time point. Statistical analysis was performed on these values. D → P indicates selected equidistant regions within the graft, from distal to proximal.

GRANULATION TISSUE AND INFLAMMATION SIGNIFICANTLY REDUCES OVER TIME. The formation of granulation tissue is an expected outcome for any implanted material. What dictates implant survival, however, is the way this tissue resolves and the extent of ECM deposition and vascularization in the long term (27,28). Quantification of the granulation tissue area surrounding the silk grafts confirmed formation of a substantial adventitial layer at 3 weeks, which is reduced at later time points where only a thin layer of cells and matrix is visible (**Figures 7A and 7C**). Caspase-3 immunostaining confirmed apoptotic cells within the granulation tissue, particularly at early time points (Supplemental Figure 5B), also reducing over time. Staining of $CD68^{+}$ macrophages further demonstrated an initial inflammatory response at 3 weeks (**Figures 7B and 7D**), significantly reduced at later time points, suggesting resolution of the acute inflammatory response. Immunostaining for vimentin, an established marker for fibroblasts, showed an abundance of fibroblasts in the granulation tissue (Supplemental Figure 8). Staining for collagen, elastin, and proteoglycans confirmed the presence of collagen alone in the granulation tissue, with no elastin or proteoglycan visible, which is suggestive of a late-stage fibroblast-mediated matrix deposition (28). CD34, a marker for progenitor endothelial cells, staining also revealed the extent of neovessel formation in the granulation tissue surrounding the silk grafts, as neovessel formation is propagated by circulating endothelial progenitor cells (29). The fluorescence images clearly demonstrate extensive neovessel staining as early as 3 weeks, which is maintained at all later time points (Supplemental Figure 3C). Collectively, these results show an initial foreign body response to the silk graft at early time points; however, positive remodeling and resolution of the acute inflammatory response suggest that the grafts are extremely well tolerated in the mid-term.

DISCUSSION

Over the past decades, there have been various approaches to the fabrication of an artificial blood vessel, particularly for small diameter applications where current surgical intervention relies entirely on autologous grafts. Several groups have reported unique bioengineering techniques that demonstrate potential in in vitro assays and preclinical animal models with modest results in human trials of hemodialysis access. Although these approaches are promising, they nevertheless fail to fulfill all the requirements of a synthetic conduit—good mechanical properties and blood compatibility while simultaneously enhancing endothelial cell migration and proliferation. Furthermore, for widespread translation to the clinic, a synthetic vascular graft should ideally be cost-effective, cell-free, with an easy and scalable manufacturing technique, and available in an off-the-shelf manner.

Our work is the first to describe the comprehensive in vivo performance of an electrospun small diameter silk vascular graft generated from and cross-linked using only water. Previous studies demonstrating the potential of silk as a graft material have used fiber winding, braiding, and gel-spinning techniques, leading to suboptimal mechanical properties (13). Long-term evaluation of a combination graft made from plaited silk fibers and wound cocoon filaments showed 85% patency at 1-year and replacement of the graft material with collagen over time (30). Together, these previous studies demonstrate the promising biological and physical properties of silk, manufactured in a way that precludes ready clinical translation. Herein, we demonstrate that electrospun silk can be engineered to have appropriate mechanical properties in a scalable, chemical-free process, while demonstrating favorable endothelial cell and blood compatibilities. In vivo performance of electrospun silk grafts was assessed in a rat model of abdominal aortic replacement at 3, 6, 12, and 24 weeks, showing high graft survival, near complete endothelial cell coverage by 6 weeks, and concomitant smooth muscle cell stabilization and contraction. Comprehensive assessment of inflammatory and remodeling cell types, and newly deposited ECM proteins, further suggests positive remodeling of the silk grafts over time and demonstrates a high degree of in vivo compatibility.

The use of silk, a natural polymer, as a biomaterial for vascular graft engineering has implicit advantages over many competing synthetic polymer-based approaches. Although synthetic polymers impart strength to a biomaterial, they generally have poor cellular compatibility, with many of the degradation products eliciting adverse immune responses in vivo (1,17). Of the natural polymers, silk is of particular interest due to its well-established strength, low immune response, controlled degradability in vivo, and versatility of manufacture (12). For these reasons, the utility of electrospun silk as a biomaterial has been well studied. Previous work on electrospun silk has established some of the important production parameters that control the mechanical properties of this material and demonstrated favorable endothelial cell attachment and growth (31–36). However, no comprehensive preclinical assessment of highly purified electrospun silk conduits has yet been carried out.

FIGURE 6 **Histologic Assessment of Neointima Formation and SMC Phenotype in Silk Grafts**

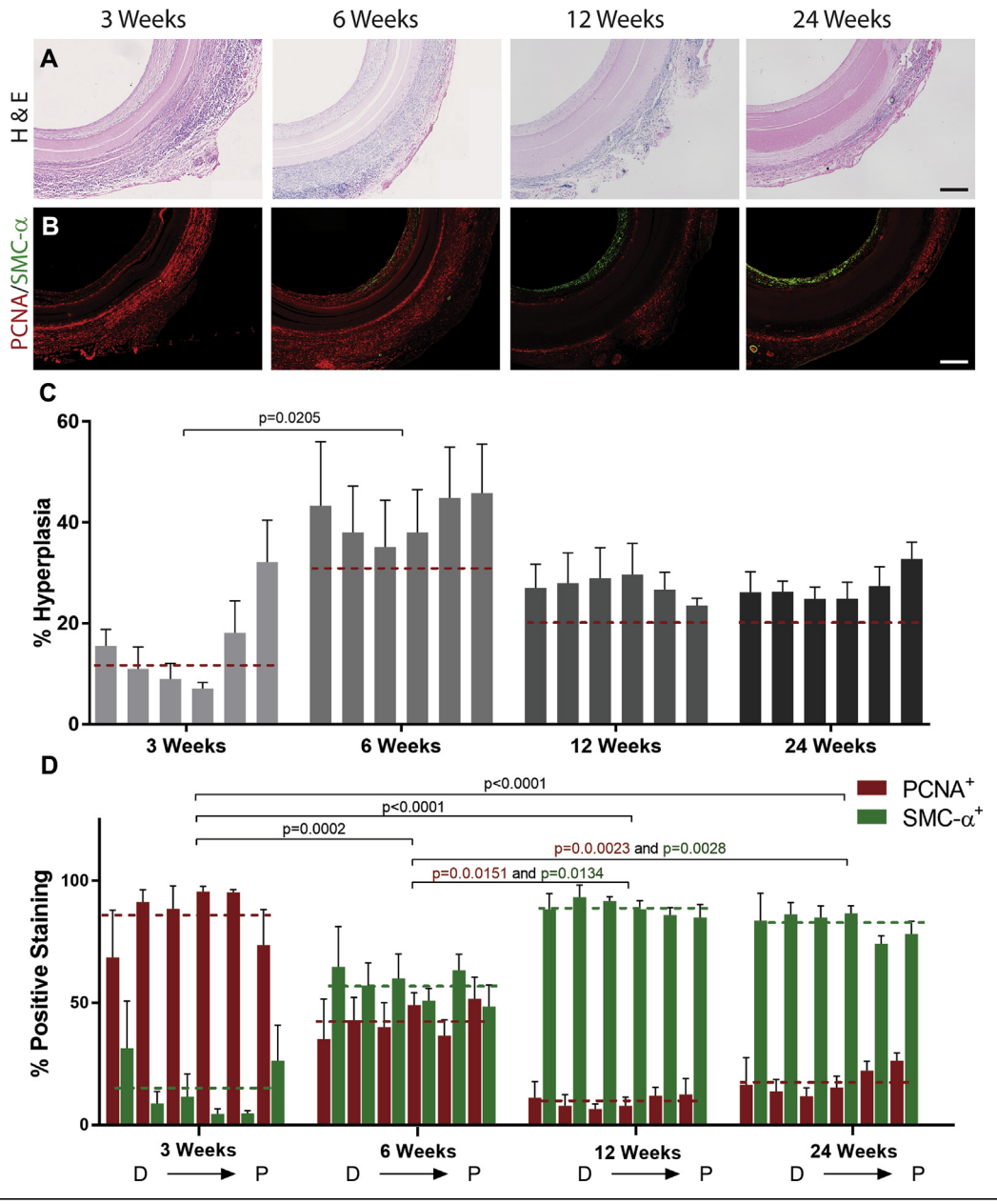

(A) Representative micrograph images of hematoxylin and eosin (H&E) staining of silk grafts at all time points. Scale bar = 200 μm. **(B)** Representative fluorescent micrograph image of proliferating cell nuclear antigen (PCNA)/smooth muscle cell actin (SMC-α) double stain at all explantation time points. Scale bar = 200 μm. **(C)** Quantification of neointima, represented as a percentage of total lumen size for each graft. N = 4 animals per time point with 3 images analyzed per region per graft. **(D)** Quantification of positive PCNA **(red)** and SMC-α **(green)** staining, represented as a percentage of the total positive staining in each graft section. N = 4 animals per time point with 3 images analyzed per region per graft. The **dashed lines** indicate the average neointima values **(C)** and average PCNA and SMC-α actin staining **(D)** for each time point. Statistical analysis was performed on these values. D → P indicates selected equidistant regions within the graft, from distal to proximal.

In this work, we fully characterized the mechanical properties of the electrospun silk, showing it to be significantly more elastic than the ePTFE. Other mechanical endpoints such as ultimate tensile strength demonstrated that although silk is not as strong as ePTFE, it is more closely matched to the native rat aorta, substantially reducing problematic compliance mismatch. Graft-specific properties, such as burst

FIGURE 7 Granulation Tissue Response and Immune Cell Accumulation in the Adventitia of Silk Grafts

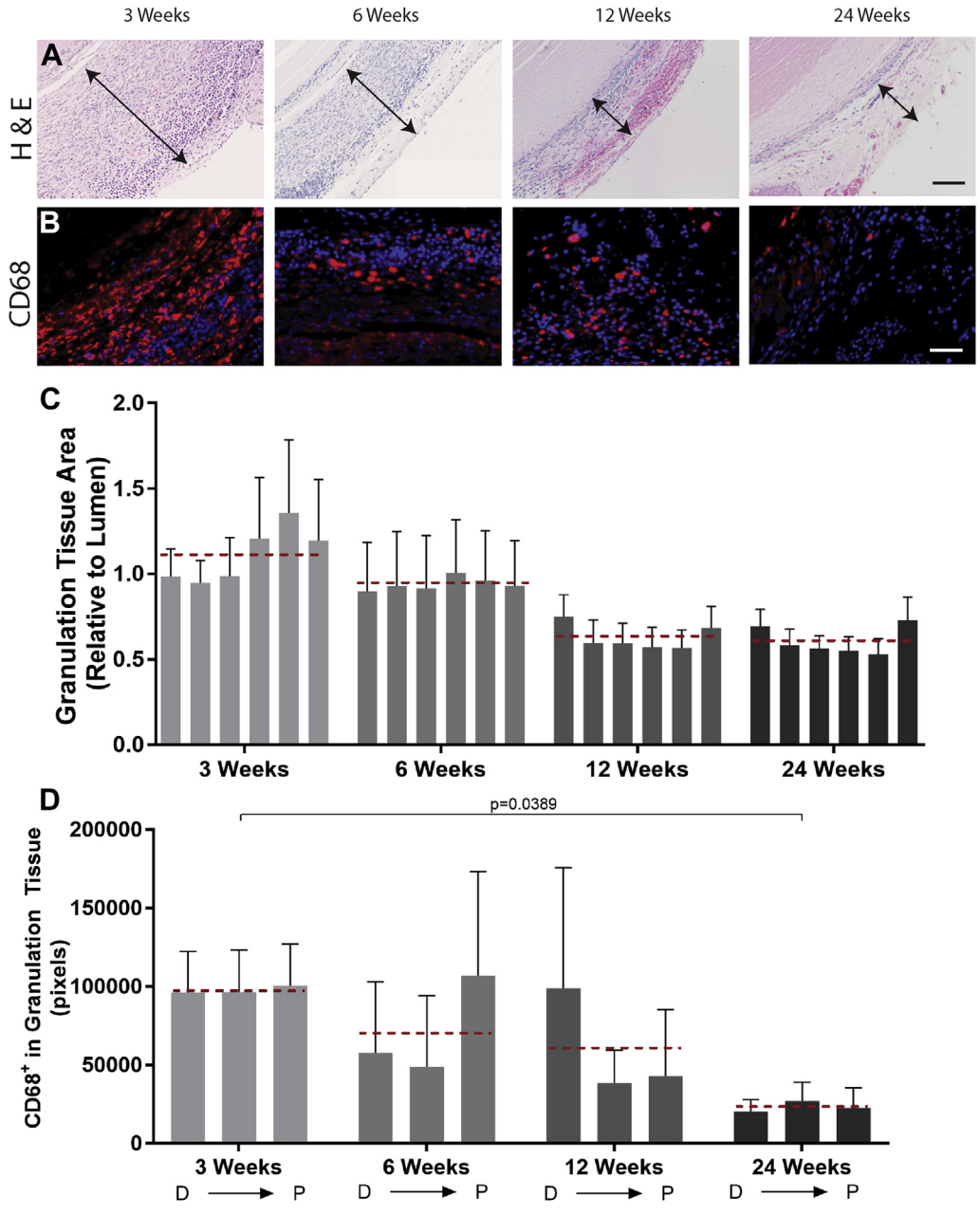

(A) Representative micrograph images of hematoxylin and eosin (H&E) staining of the adventitia surrounding the silk grafts at all time points. Scale bar = 100 μm. **(B)** Representative fluorescent micrograph images of CD68 immunostaining at all time points. Scale bar = 100 μm. **(C)** Quantification of granulation tissue area, represented as a percentage of total lumen size for each graft. N = 4 animals per time point with 3 images analyzed per region per graft. **(D)** Quantification of positive CD68 staining, indicating macrophage presence, in the granulation tissue area, represented as a percentage of total granulation tissue for each section. N = 4 animals per time point with 3 images analyzed per region per graft. CD68 staining is **red,** and 4′,6-diamidino-2-phenylindole staining is **blue.** Scale bar = 100 μm. The **red dashed lines** indicate the average granulation tissue thickness values **(C)** and average CD68 staining **(D)** for each time point. Statistical analysis was performed on these values. D → P indicates selected equidistant regions within the graft, from distal to proximal.

pressure, revealed that the silk grafts could withstand internal pressures of 849 mm Hg, which is well above physiological values and outperforms other electrospun silk tubes previously described (31,32,34). Furthermore, the silk grafts withstood a suture pull-out strength of 0.86 N, which is within the range of previously published results for small-diameter polymer-based poly(glycerol sebacate) and polycaprolactone grafts that were also implanted into the rat abdominal aorta position (15).

Biological compatibility of the silk materials was shown here to be favorable for use as a vascular graft material. Specifically, endothelial cells interacted well with the electrospun silk, with cells attaching and proliferating well on the surface of the scaffolds, forming a complete and functional monolayer evident by the expression of vascular endothelial cadherin. Another crucial factor for graft patency is the blood compatibility of the material, an aspect commonly overlooked. In this work, we describe the striking blood compatibility of electrospun silk scaffolds. We demonstrate a significantly reduced fibrin network formation on silk, when compared with other electrospun scaffolds (PCL) and the clinical control ePTFE. Furthermore, whole blood contact displayed less clot formation on the silk scaffolds with negligible red blood cell attachment visible under scanning electron microscopy.

In vivo implantation of an electrospun silk graft has not before been reported, with previous in vivo studies being performed with woven silk and gel spun silk tubes. Gel-spun small-diameter grafts were manufactured by winding silk fibers onto a cylindrical mandrel to create highly porous conduits for short-term studies in rats. Initial findings demonstrated significant levels of SMC hyperplasia, leading some investigators to suggest further optimization of mechanical properties, and subsequent modification of the silk may be necessary to limit SMC proliferation (37,38). A separate approach utilized unmodified, knitted silk to engineer small-diameter grafts; however, this manufacturing approach resulted in material strength and compliance insufficient for in vivo evaluation in pre-clinical models (30,39–41).

In a rat model of abdominal aortic replacement, our electrospun silk graft enabled rapid coverage of the graft lumen, contrary to ePTFE, which remained largely uncovered, even at 24 weeks. Immunohistochemistry confirmed the presence of endothelial cells as early as 3 weeks, with an almost compete monolayer forming by 6 weeks. Further histologic analysis of the neointima formation and composition over time suggests a stabilization of neointima from 6 weeks, with regression of total neointima accompanied by the increased collagen, elastin, and proteoglycan production. A phenotypic switch of the cells in the hyperplasia to less proliferative, SMC-α expressing cells further supports this. Furthermore, positive remodeling of the silk graft was observed, with the formation of a thin, collagen rich capsule with extensive neovessel formation. The influence of a healthy endothelium in blood vessels is widely recognized, with past studies establishing the importance of endothelial-derived molecules such as nitric oxide in the regulation of SMC proliferation and maintenance of vessel patency (42). Our results similarly suggest the benefit of a rapidly endothelialized lumen, which may responsible for the observed stabilization of hyperplasia progression observed from 6 weeks.

CONCLUSIONS

In this work, we evaluate the mechanical and biological properties of an electrospun silk graft, demonstrating the feasibility of engineering an entirely cell-free, synthetic scaffold with mechanical properties similar to native vessel tissue. Furthermore, the ability to favorably interact with endothelial cells in vitro while resisting clot formation further supports the use of this material as a vascular graft. We show, for the first time, the in vivo performance of an electrospun silk scaffold in a rat model of abdominal aortic replacement for up to 6 months. Our results show early endothelial cell interaction and near complete luminal coverage by 6 weeks post-implantation. Further analysis into the matrix and cellular composition of the hyperplasia and adventitial tissues reveals clinically relevant regression from 6 weeks onward, suggesting the stabilization of the neointima and positive remodeling of the silk graft. Collectively, our results illustrate the promise for electrospun silk conduits to be used as small diameter vessels, representing a cell-free and cost-effective option for small diameter synthetic grafts in clinical use. These results justify further exploration in larger preclinical animal models to evaluate long-term graft survival and stability.

ACKNOWLEDGMENTS The authors acknowledge the facilities as well as scientific and technical assistance at the Australian Center for Microscopy and Microanalysis, The University of Sydney.

ADDRESS FOR CORRESPONDENCE: Dr. Steven G. Wise, The Heart Research institute, 7 Eliza Street Newtown, New South Wales 2042, Australia. E-mail: steve.wise@hri.org.au. OR Dr Jelena Rnjak-Kovacina, Graduate School of Biomedical Engineering, University of New South Wales, Sydney, New South Wales 2052, Australia. E-mail: j.rnjak-kovacina@unsw.edu.au.

PERSPECTIVES

COMPETENCY IN MEDICAL KNOWLEDGE: Clinical applications for small diameter (<6 mm) arterial bypass grafting include coronary artery bypass graft and peripheral vascular applications. The 2 clinically available synthetic graft materials, polyethylene terephthalate (Dacron) and ePTFE produce an unfavorable immune response and are highly thrombogenic, making them innately unsuitable for vascular implantation. New synthetic graft materials with improved efficacy have long been required. This study demonstrates the potential of synthetic silk conduits as off-the-shelf small-diameter grafts.

TRANSLATIONAL OUTLOOK: There is currently a large unmet need for synthetic small-diameter vascular grafts that are effective in small-diameter applications. Small-diameter, cell-free, electrospun silk grafts were shown here to remain patent for up to 6 months in a preclinical rat model of aortic replacement, with results suggesting almost complete endothelialization and neointimal hyperplasia stabilization as early as 6 weeks. Positive remodeling over time also suggests the potential for improved biointegration. Further in vivo studies in larger animal models would be necessary to validate the use of electrospun silk scaffolds in models that also evaluate other aspects important to graft patency in humans such as long-term graft survival.

REFERENCES

1. Seifu DG, Purnama A, Mequanint K, Mantovani D. Small-diameter vascular tissue engineering. Nat Rev Cardiol 2013;10:410–21.

2. Pashneh-Tala S, MacNeil S, Claeyssens F. The tissue-engineered vascular graft-past, present, and future. Tissue Eng Part B Rev 2015 Oct 8 [E-pub ahead of print].

3. Dahl SL, Kypson AP, Lawson JH, et al. Readily available tissue-engineered vascular grafts. Sci Transl Med 2011;3:68ra9.

4. L'Heureux N, Dusserre N, Konig G, et al. Human tissue-engineered blood vessels for adult arterial revascularization. Nat Med 2006;12:361–5.

5. L'Heureux N, Paquet S, Labbe R, Germain L, Auger FA. A completely biological tissue-engineered human blood vessel. FASEB J 1998; 12:47–56.

6. McAllister TN, Maruszewski M, Garrido SA, et al. Effectiveness of haemodialysis access with an autologous tissue-engineered vascular graft: a multicentre cohort study. Lancet 2009;373: 1440–6.

7. Niklason LE, Gao J, Abbott WM, et al. Functional arteries grown in vitro. Science 1999;284: 489–93.

8. Quint C, Arief M, Muto A, Dardik A, Niklason LE. Allogeneic human tissue-engineered blood vessel. J Vasc Surg 2012;55:790–8.

9. Lawson JH, Glickman MH, Ilzecki M, et al. Bioengineered human acellular vessels for dialysis access in patients with end-stage renal disease: two phase 2 single-arm trials. Lancet 2016;387: 2026–34.

10. Kannan RY, Salacinski HJ, Butler PE, Hamilton G, Seifalian AM. Current status of prosthetic bypass grafts: a review. J Biomed Mater Res B Appl Biomater 2005;74:570–81.

11. Santerre JP, Woodhouse K, Laroche G, Labow RS. Understanding the biodegradation of polyurethanes: from classical implants to tissue engineering materials. Biomaterials 2005;26: 7457–70.

12. Rockwood DN, Preda RC, Yucel T, Wang X, Lovett ML, Kaplan DL. Materials fabrication from *Bombyx mori* silk fibroin. Nat Protoc 2011;6:1612–31.

13. Thurber AE, Omenetto FG, Kaplan DL. In vivo bioresponses to silk proteins. Biomaterials 2015; 71:145–57.

14. Vepari C, Kaplan DL. Silk as a biomaterial. Prog Polym Sci 2007;32:991–1007.

15. Wu W, Allen RA, Wang Y. Fast-degrading elastomer enables rapid remodeling of a cell-free synthetic graft into a neoartery. Nat Med 2012; 18:1148–53.

16. Pektok E, Nottelet B, Tille JC, et al. Degradation and healing characteristics of small-diameter poly(epsilon-caprolactone) vascular grafts in the rat systemic arterial circulation. Circulation 2008; 118:2563–70.

17. de Valence S, Tille JC, Mugnai D, et al. Long term performance of polycaprolactone vascular grafts in a rat abdominal aorta replacement model. Biomaterials 2012;33:38–47.

18. Laube HR, Duwe J, Rutsch W, Konertz W. Clinical experience with autologous endothelial cell-seeded polytetrafluoroethylene coronary artery bypass grafts. J Thorac Cardiovasc Surg 2000;120:134–41.

19. Higgins SP, Solan AK, Niklason LE. Effects of polyglycolic acid on porcine smooth muscle cell growth and differentiation. J Biomed Materials Res A 2003;67:295–302.

20. Kristofik NJ, Qin L, Calabro NE, et al. Improving in vivo outcomes of decellularized vascular grafts via incorporation of a novel extracellular matrix. Biomaterials 2017;141:63–73.

21. Wise SG, Liu H, Kondyurin A, et al. Plasma ion activated expanded polytetrafluoroethylene vascular grafts with a covalently immobilized recombinant human tropoelastin coating reducing neointimal hyperplasia. ACS Biomater Sci Eng 2016;2:1286–97.

22. McDonald A, Iruela-Arispe ML. Healing arterial ulcers: endothelial lining regeneration upon vascular denudation injury. Vascul Pharmacol 2015;72:9–15.

23. Chaabane C, Otsuka F, Virmani R, Bochaton-Piallat ML. Biological responses in stented arteries. Cardiovasc Res 2013;99:353–63.

24. Farb A, Kolodgie FD, Hwang JY, et al. Extracellular matrix changes in stented human coronary arteries. Circulation 2004;110:940–7.

25. Beamish JA, He P, Kottke-Marchant K, Marchant RE. Molecular regulation of contractile smooth muscle cell phenotype: implications for vascular tissue engineering. Tissue Eng Part B Rev 2010;16:467–91.

26. Rensen SS, Doevendans PA, van Eys GJ. Regulation and characteristics of vascular smooth muscle cell phenotypic diversity. Neth Heart J 2007;15:100–8.

27. Ratner BD, Bryant SJ. Biomaterials: where we have been and where we are going. Annu Rev Biomed Eng 2004;6:41–75.

28. Anderson JM. Biological responses to materials. Annu Rev Mater Res 2001;31:81–110.

29. Masuda H, Asahara T. Post-natal endothelial progenitor cells for neovascularization in tissue regeneration. Cardiovasc Res 2003;58:390–8.

30. Enomoto S, Sumi M, Kajimoto K, et al. Long-term patency of small-diameter vascular graft

made from fibroin, a silk-based biodegradable material. J Vasc Surg 2010;51:155–64.

31. Catto V, Fare S, Cattaneo I, et al. Small diameter electrospun silk fibroin vascular grafts: mechanical properties, in vitro biodegradability, and in vivo biocompatibility. Mater Sci Eng C Mater Biol Appl 2015;54:101–11.

32. Marelli B, Achilli M, Alessandrino A, et al. Collagen-reinforced electrospun silk fibroin tubular construct as small calibre vascular graft. Macromol Biosci 2012;12:1566–74.

33. Marelli B, Alessandrino A, Fare S, Freddi G, Mantovani D, Tanzi MC. Compliant electrospun silk fibroin tubes for small vessel bypass grafting. Acta Biomater 2010;6:4019–26.

34. Soffer L, Wang X, Zhang X, et al. Silk-based electrospun tubular scaffolds for tissue-engineered vascular grafts. J Biomater Sci Polym Ed 2008;19:653–64.

35. Zhang X, Baughman CB, Kaplan DL. In vitro evaluation of electrospun silk fibroin scaffolds for vascular cell growth. Biomaterials 2008;29:2217–27.

36. Zhang X, Wang X, Keshav V, et al. Dynamic culture conditions to generate silk-based tissue-engineered vascular grafts. Biomaterials 2009;30:3213–23.

37. Lovett M, Eng G, Kluge JA, Cannizzaro C, Vunjak-Novakovic G, Kaplan DL. Tubular silk scaffolds for small diameter vascular grafts. Organogenesis 2010;6:217–24.

38. Lovett ML, Cannizzaro CM, Vunjak-Novakovic G, Kaplan DL. Gel spinning of silk tubes for tissue engineering. Biomaterials 2008;29:4650–7.

39. Aytemiz D, Sakiyama W, Suzuki Y, et al. Small-diameter silk vascular grafts (3 mm diameter) with a double-raschel knitted silk tube coated with silk fibroin sponge. Adv Healthc Mater 2013;2:361–8.

40. Nakazawa Y, Sato M, Takahashi R, et al. Development of small-diameter vascular grafts based on silk fibroin fibers from *Bombyx mori* for vascular regeneration. J Biomater Sci Polym Ed 2011;22:195–206.

41. Yagi T, Sato M, Nakazawa Y, et al. Preparation of double-raschel knitted silk vascular grafts and evaluation of short-term function in a rat abdominal aorta. J Artif Organs 2011;14:89–99.

42. Melchiorri AJ, Hibino N, Fisher JP. Strategies and techniques to enhance the in situ endothelialization of small-diameter biodegradable polymeric vascular grafts. Tissue Eng Part B Rev 2013;19:292–307.

KEY WORDS rat aortic interposition, silk, small diameter, vascular graft

APPENDIX For supplemental figures, please see the online version of this paper.